Determination of Layers' Thicknesses by Spectral Analysis of Swept-Frequency Measurement Signals

著者	Weiying Cheng, Hidetoshi Hashizume
journal or publication title	IEEE sensors journal : a publication of the IEEE Sensors Council
volume	20
number	15
page range	8643-8655
year	2020-08-01
URL	http://hdl.handle.net/10097/00135604

doi: 10.1109/JSEN.2020.2982944

Determination of Layers' Thicknesses by Spectral Analysis of Swept-Frequency Measurement Signals

Weiying Cheng and Hidetoshi Hashizume

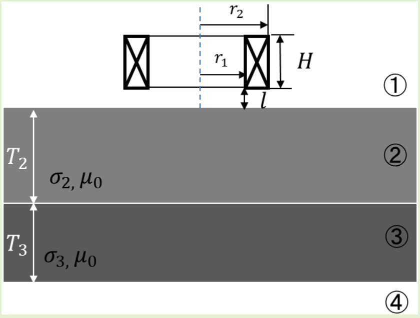

***Abstract*—The aim of this study was to investigate the use of swept frequency eddy current testing to measure each layer's thickness in a layered structure. Theoretical inference showed the impedance signal is an integrand of shape function and generalized reflection function. Analytical study indicated that the wavelength to maximize the shape function is an indicator of a probe's thickness measurement ability. Comprehensive investigation revealed the reflection coefficient of a layered structure could be considered a modification of that of a half space. The amount of modification is a logarithmic linear function of plate thickness and thus a characteristic feature for thickness estimation. The frequency response of a double-layered structure depends, in addition to layer-wise thickness and properties, significantly on the relation of the conductivities of the two layers. In order to evaluate two closely attached layers, we introduced a novel variable, the derivative of impedance with respect to log scaled angular frequency. Spectral analysis on impedance or the frequency derivative related quantities, such as extrema of the real or imaginary parts of the variable, suggested it is possible to determine the top layer's thickness using characteristic features taken from high frequency signals, whereas the lower layer's thickness using characteristic features taken from lower frequency signals afterwards. The characteristic quantities derived from spectral analysis are conductivity independent, implying of conductivity independent measurement. The analytical findings were experimentally verified, suggested that it is possible to determine layers' thicknesses by spectral analysis of swept frequency eddy current testing signals.**

***Index Terms*—Electromagnetic measurements, frequency domain analysis, impedance, spectral analysis, thickness measurement.**

I. INTRODUCTION

LAYERED structures are extensively used in industry and appliances [1]–[10] attributing to their excellent properties against corrosion-erosion, high level of solidity, defense in depth and etc. The mechanical and physical properties and performance of a layered structure depend significantly on each layer's thickness. A reliable thickness measurement technique is vital for layered structures' quality monitoring and maintenance [1]–[11], [15], [17].

Eddy current testing (ECT) is one of the most intensively studied technique for crack detection [9], [12]–[14] and thickness measurement [4], [6]–[8], [10], [11], [15], [17]. The ECT signal, generally the impedance change of inspection probe, reveals the interaction between probe and test object, and depends on probe geometry and setup, operating frequency, and the test object's geometry and electromagnetic properties. Because of interaction and multi-interference of electromagnetic fields, the ECT signals of a layered structure are integral of all the layers. In order to characterize the layer of interest, the interferences of other layers have to be excluded and the signals of 'this' layer are used. We can also use characteristic features that are sensitive to the particular layer but insensitive to the others.

Conventional single frequency ECT is sensitive to a certain depth of a test object according to electromagnetic theory. The pulsed eddy current testing (PECT) technique, as a time domain method, contains frequency rich information and shows promising results in layered structures characterization. However, Fourier transform and other advanced

Manuscript received January 27, 2020; revised March 10, 2020; accepted March 12, 2020. The associate editor coordinating the review of this article and approving it for publication was Prof. Guiyun Tian. *(Corresponding author: Weiying Cheng.)*

Weiying Cheng is with the NDE Center, Japan Power Engineering and Inspection Corporation, Yokohama 230 0044, Japan, and also with the Quantum Science and Engineering Department, Tohoku University, Sendai 980-8577, Japan (e-mail: cheng-weiying@japeic.or.jp).

Hidetoshi Hashizume is with the Quantum Science and Engineering Department, Tohoku University, Sendai 980-8577, Japan (e-mail: author@nrim.go.jp).

Digital Object Identifier 10.1109/JSEN.2020.2982944

signal processing and interpolation are needed to abstract the characteristic features and link them with the layers [15], [16], [18]. Swept frequency eddy current testing (SFECT), as a frequency domain method, can provide information of different depths directly [6], [7], [17]. The frequency-wise response can be directly linked to the layers.

Previous studies on PECT of a pipe covered by insulation and cover sheet showed that the PECT signals of a layered structure could be decoupled to some degree in time domain [8]. The decay rate of time-varying signals is robust against the variation of a probe's liftoff and inclination and applicable to pipe wall thickness assessment. References [11] and [17] showed that the thickness of a single conductive plate or a non-conductive coating on it could be estimated by spectrum analysis of swept-frequency eddy current testing (SFECT) signals. With regard to non-ferromagnetic conducting plates of same thickness, identical $\omega\sigma$, the product of angular frequency (ω) and electrical conductivity (σ), yields identical ECT signal, whereas identical of $\omega\sigma$ is attainable by frequency sweeping. The extrema in the SFECT signals spectrum, e.g., minimum of the normalized impedance's phase or maximum of the normalized impedance's real part, are characteristic quantities for thickness evaluation. Investigation of SFECT of air-gap-separated double-layered structures [10] showed that signals of the two layers could be 'separated' in frequency domain by differential operation [10]. Thereby the top and the lower layers was characterized respectively using high frequency and low frequency signals. The differential with respect to log scaled frequency is almost invariant to the variation of air gap.

Nonetheless, many issues remain in the electromagnetic measurement of layered structures. One is probe selection. References [11] and [17] showed that the measureable thickness changes with probe. To choose a comparable probe, we need to know the probe's thickness measurement performance properly. The second is the enhancement of thickness assessment accuracy. The master curves being constructed in [11] and [17] are nonlinear. Characteristic features which are linearly correlated with thickness are sought for more accurate thickness estimation. The ultimate objective is to determine the thickness of each layer in a multilayered structure, even without knowing the layer-wise electromagnetic properties. These three issues are addressed in this paper.

We established characterization approaches on the basis of SFECT impedance signal analysis in [11] and [17]. In this study, we focused on more fundamental variables, the shape function and reflection coefficient, and constructed characterization scheme based on spectrum analysis. The findings were applied to impedance signals and verified analytically and experimentally.

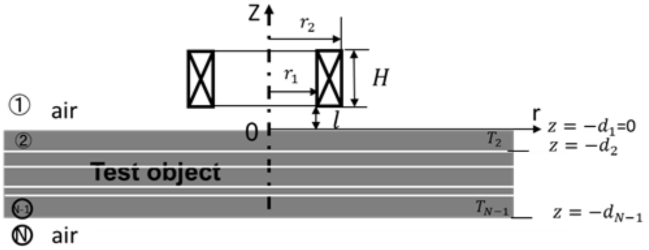

Fig. 1. Modeling of eddy current testing of a layered structure.

TABLE I
COILS USED IN ANALYTICAL STUDY

	r_1 (mm)	r_2 (mm)	l (mm)	H (mm)	n_{cd}	Wavelength (mm)
COIL-6	8	10	0.5	3	85	5.7
COIL-4	5	8	0.5	2	268	4.4

II. SHAPE FUNCTION AND A PROBE'S THICKNESS MEASUREMENT ABILITY

As stated in [10], [11], [17], [18], [21], [22], layered structures are usually modelled by planar layers in theoretical analysis. Consider of ECT using a self-induction coil (Fig. 1). The cylindrical air-cored coil (inner and outer radius r_1 and r_2, thickness H) carrying alternating current of angular frequency ω is placed on a test object with liftoff l. The change of coil impedance due to induced eddy currents can be calculated [11], [22] by

$$\begin{aligned}\Delta Z(\omega) &= \Delta R + j\omega\Delta L \\ &= j2\pi\omega\mu_0 n_{cd}^2 \int_0^\infty \frac{\chi^2(\lambda_0 r_1, \lambda_0 r_2)}{\lambda_0^6} \\ &\quad \times \left(e^{-\lambda_0 l} - e^{-\lambda_0(l+H)}\right)^2 R(\lambda_0)\, d\lambda_0, \qquad (1)\end{aligned}$$

where μ_0 is the magnetic permeability of free space, n_{cd} the turn density of the coil. λ_0, the integral parameter of the Bessel function, is also considered as wavenumber [11], [12]. In the integrand, $R(\lambda_0)$ is the reflection coefficient relevant to test object [10]–[14], while $\frac{\chi^2(\lambda_0 r_1, \lambda_0 r_2)}{\lambda_0^6}\left(e^{-\lambda_0 l} - e^{-\lambda_0(l+H)}\right)^2$, the shape function $S(\lambda_0)$, solely depend on geometry and setup of the probe coil. The rewritten of (1),

$$\Delta Z(\omega) = j2\pi\omega\mu_0 n_{cd}^2 \int_0^\infty S(\lambda_0)\, R(\lambda_0)\, d\lambda_0, \qquad (2)$$

indicates that the impedance signal is the integration of shape function $S(\lambda_0)$ and reflection coefficient $R(\lambda_0)$.

The shape functions of the air-cored coils used in [11] and [17], which are denoted respectively as COIL-6 and COIL-4 in this paper, were calculated and correlated with the thickness measurement ability. Table I is a list of the specifics. The shape functions plotted in Fig. 2 shows the change of shape function with wavenumber. $S(\lambda_0)$ of COIL-4 and COIL-6 respectively reaches maximum at wavenumbers 220.83 (1/meter) and 176. 66 (1/meter), indicating that a probe of particular dimension maximizes impedance signal at a particular wavenumber. The correspondent wavelengths (1/wavenumber) are 4.4mm and 5.7mm, respectively. Fig. 2(a) in [17] showed that COIL-4 is able to measure up to 4mm thick conducting plates, and Fig. 5 in [11] showed COIL-6 is able to measure up to 6mm thick plate. Note that the measurable thickness is almost equivalent to the wavelength that maximizes the shape function, suggesting the wavelength an indicator of a coil's thickness measurement

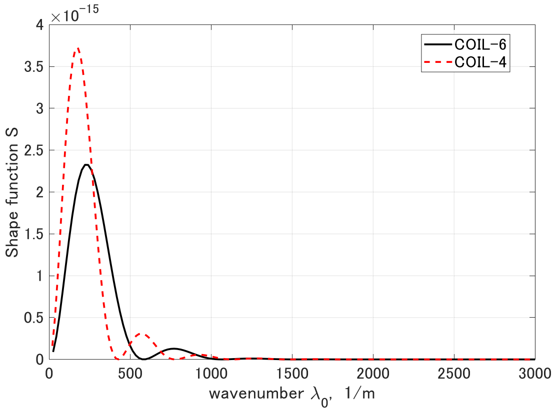

Fig. 2. Change of the shape function value with wavenumber.

ability. In other words, we should choose a probe whose shape function is maximized at a wavelength longer than a given object's thickness.

III. THE GENERALIZED REFLECTION COEFFICIENT $\tilde{R}_{12}$

The reflection coefficient $R(\lambda_0)$ is decided by multi- transmission and reflection of electromagnetic waves between layers.

Fig. 1 shows the ECT measurement of an *N-2* layer structure that the probe is placed in region 1 (air); regions 2 to *N-1* are the *N-2* layers; region *N* is air below the structure. The z coordinate of the top layer is set to 0, and the z coordinate of the interface between regions i and $i+1$ is denoted by $-d_i$, thus the thickness of the *ith* layer, T_i, equals to $d_{i+1} - d_i$. Waves generated by excitation coil in region 1 incident to the test object, transmit and reflect in the layers, a portion of the waves finally go back to region 1 and being received by pickup coil.

Under the assumption that the material in each region is liner, homogenous and isotropic, and the wave propagates in the z direction, the transmission and reflection coefficients at the interface of the i$^{\text{th}}$ and the (i+1)$^{\text{th}}$ regions are respectively [18], [20],

$$\mathrm{T}_{i,i+1} = \frac{2\mu_{i+1}k_{iz}}{\mu_{i+1}k_{iz} + \mu_i k_{i+1,z}}$$

and

$$R_{i,i+1} = \frac{\mu_{i+1}k_{i,z} - \mu_i k_{i+1,z}}{\mu_{i+1}k_{iz} + \mu_i k_{i+1,z}} \tag{3}$$

where μ is the magnetic permeability, $k = \sqrt{\lambda_0^2 + j\omega\mu\sigma}$, σ is the conductivity and ω the angular frequency. The generalized reflection coefficient at the interface of the i$^{\text{th}}$ and the (i+1)$^{\text{th}}$ regions is

$$\tilde{R}_{i,i+1} = \frac{R_{i,i+1} + \tilde{R}_{i+1,i+2}e^{-2k_{i+1}T_i}}{1 + R_{i,i+1}\tilde{R}_{i+1,i+2}e^{-2k_{i+1}T_i}}, \tag{4}$$

where $\tilde{R}_{i+1,i+2}$ stands for subsurface reflection.

After multi- transmission and reflection, part of the waves is received by the pickup probe in region 1. Therefore, $\tilde{R}_{1,2}$, the generalized reflection coefficient at the interface of regions 1 and 2, is equivalent to the $R(\lambda_0)$ in (1) and (2).

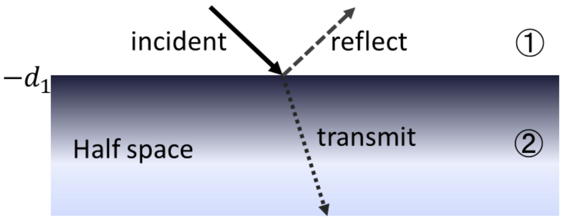

Fig. 3. Reflection and transmission of plane wave in eddy current measurement of a half space.

Without reflection between the N$^{\text{th}}$ and the hypothetical (N + 1)$^{\text{th}}$ regions, $\tilde{R}_{N,N+1} = 0$, $\tilde{R}_{i,i+1}$ and eventually the $\tilde{R}_{1,2}$ can be solved recursively.

The reflection coefficient provides insight into the ECT of layered structures and directly reveals the correlation between physics variables. The impedance is the integrand of shape function and generalized reflection coefficient $\tilde{R}_{1,2}$.

From simplicity to complexity, hereafter we investigated the $\tilde{R}_{1,2}$ of ECT measurement of a half space, a single plate, and a two-plate stack and found out characteristic quantities which are linearly correlated with thickness. In sequence the structure of the latter is more complicated than that of the former, and the reflection coefficient of the latter is considered as a modification of that of the former.

A. Conductive Half Space

Fig. 3 shows the reflection and transmission of plane waves in ECT measurement of a half space: a portion of the incident waves reflect at the interface and the left transmit into the half space (region 2). Without reflection in region 2, the generalized reflection coefficient $\tilde{R}_{1,2}$ is equal to the reflection coefficient $R_{1,2}$. By the way, in region 1, $\sigma_1 = 0$ and $\mu_1 = \mu_0$, hence $k_1 = \lambda_0$, and $\tilde{R}_{1,2} = R_{1,2} = \frac{\mu_2 k_1 - \mu_1 k_2}{\mu_2 k_1 + \mu_1 k_2} = \frac{\mu_2\lambda_0 - \mu_0 k_2}{\mu_2\lambda_0 + \mu_0 k_2}$, where $k_2 = \sqrt{\lambda_0^2 + j\omega\mu_2\sigma_2}$. For non-ferromagnetic materials, $\mu_2 = \mu_0$, thus

$$\tilde{R}_{1,2} = \frac{\lambda_0 - k_2}{\lambda_0 + k_2} = \frac{-j\omega\mu_0\sigma_2}{(\lambda_0 + k_2)^2}. \tag{5}$$

The square term in the dominator and the negative sign in the numerator of $\tilde{R}_{1,2}$ in (5) demonstrate the fact that the reflection is opposite to the incident. Equation (5) also reveals that $\tilde{R}_{1,2}$ depends on the relative magnitudes of $j\omega\mu_0\sigma_2$ and λ_0. The amplitude of $\tilde{R}_{1,2}$ is small for poor conductors, or when the measurement is carried out at low frequencies. In contrast, $\tilde{R}_{1,2}$ is large for good conductors or high frequency measurements. When $j\omega\mu_0\sigma_2 \gg \lambda_0^2$, $\tilde{R}_{1,2} \cong -1$, indicates nearly total reflection of the incident wave. Large $|\tilde{R}_{12}|$ also means large signal and highly sensitive measurement. The forgoing analysis also supports the general knowing that ECT is applicable to good conductors and prefer to be carried out at high frequencies.

B. A Single Plate and Characteristic Quantities Linearly Correlated With Plate Thickness

Fig. 4 shows ECT of a conducting plate of thickness T_2 that

$$\tilde{R}_{1,2} = \frac{R_{1,2} + \tilde{R}_{2,3}e^{-2k_2T_2}}{1 + R_{1,2}\tilde{R}_{2,3}e^{-2k_2T_2}}, \tag{6}$$

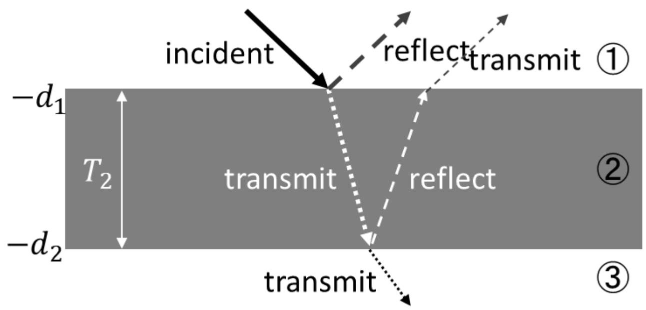

Fig. 4. Reflection and transmission of plane wave in eddy current measurement of a single plate.

where $R_{1,2}$ is equal to the generalized reflection coefficient of a half space. In other words, the $\tilde{R}_{1,2}$ of a plate is a modification of that of a half space. $\tilde{R}_{2,3}e^{-2k_2T_2}$ changes with plate thickness and diminishes to 0 when $T_2 \to \infty$, suggesting of emulating a half space using a sufficiently thick plate.

Taking into consideration that $\tilde{R}_{2,3} = R_{2,3} = -R_{1,2}$, (6) is modified to

$$\tilde{R}_{1,2} = \frac{R_{1,2} - R_{1,2}e^{-2k_2T_2}}{1 - R_{1,2}^2 e^{-2k_2T_2}}. \tag{7}$$

The $|R_{1,2}^2 e^{-2k_2T_2}|$ in the dominator is always smaller than 1. If $|R_{1,2}^2 e^{-2k_2T_2}| \ll 1$, Taylor expanding of $\tilde{R}_{1,2}$ yields

$$\begin{aligned}\tilde{R}_{1,2} &= R_{1,2}\left(1 - e^{-2k_2T_2}\right)\left(1 + R_{1,2}^2 e^{-2k_2T_2} + R_{1,2}^4 e^{-4k_2T_2} + \ldots\right)\\ &= R_{1,2} - R_{1,2}e^{-2k_2T_2} + R_{1,2}^3 e^{-2k_2T_2} - R_{1,2}^3 e^{-4k_2T_2} + \ldots\end{aligned} \tag{8}$$

Therefore, the modification of the generalized reflection coefficient from a half space to that of a single plate is approximately (T_2 is denoted as T for simplicity)

$$\begin{aligned}\Delta\tilde{R}_{1,2} &= \tilde{R}_{1,2} - R_{1,2}\\ &= -R_{1,2}e^{-2k_2T} + R_{1,2}^3 e^{-2k_2T} - R_{1,2}^3 e^{-4k_2T} + \ldots\\ &\cong -R_{1,2}\left(1 - R_{1,2}^2\right)e^{-2k_2T}.\end{aligned} \tag{9}$$

Noting in polar complex form,

$$-R_{1,2}\left(1 - R_{1,2}^2\right) = \left|R_{1,2}\left(1 - R_{1,2}^2\right)\right| e^{j\theta},$$

and

$$e^{-2k_2T} = |e^{-2k_2T}|e^{j\beta}, \tag{10}$$

hence

$$\Delta\tilde{R}_{1,2} = \left|\Delta\tilde{R}_{1,2}\right| \mathrm{e}^{\mathrm{j}\alpha} = \left|R_{1,2}\left(1 - R_{1,2}^2\right)\right| |e^{-2k_2T}| e^{j\theta} e^{j\beta}, \tag{11}$$

where $\left|\Delta\tilde{R}_{1,2}\right|$, $\left|R_{1,2}\left(1 - R_{1,2}^2\right)\right|$ and $|e^{-2k_2T}|$ are modulus of complex numbers that

$$\left|\Delta\tilde{R}_{1,2}\right| = \left|R_{1,2}\left(1 - R_{1,2}^2\right)\right| |e^{-2k_2T}|, \tag{12}$$

where $R_{1,2}\left(1 - R_{1,2}^2\right)$ is determined by operating frequency and the plate's electromagnetic properties. The arguments of complex numbers, $\alpha = \arg\left(\Delta\tilde{R}_{1,2}\right)$, $\theta = \arg(R_{1,2}\left(1 - R_{1,2}^2\right))$ and $\beta = \arg(e^{-2k_2T})$ satisfy $\alpha = \theta + \beta$.

$|\Delta\tilde{R}_{1,2}|$ in log scale, $\ln|\left(\Delta\tilde{R}_{1,2}\right)| \approx [\ln|(R_{12})((1 - R_{12}^2)| - 2k_2T$, is approximately a linear function of thickness T, whereas $2k_2$, the slope of the linear plot, varies with material property and frequency. The identical of the phase angles, $\alpha = \theta + \arg(e^{-2k_2T})$, shows that the phase of $\Delta\tilde{R}_{1,2}, \alpha$, is also a linear function of thickness T. θ is a constant decided by material property and frequency.

Hereinabove linear relation has been confirmed by following analytical examples. The assumed ECT measurements were conducted by COIL-6 on non-ferromagnetic conducting plates made of material '***A***' (conductivity 10MS/m). The presumed plates are sufficiently large that edge effect is negligible. The 1, 2, 3, 4, 5 mm thick '***A***' plates are respectively denoted by 'A', 'AA', 'AAA', 'AAAA' and 'AAAAA' (one letter represents 1mm, the same hereinafter). The liftoff is 0.5mm, and the frequency sweeps from 20Hz to 300 kHz, with 60 discrete frequencies in regular interval of log scale.

The generalized reflection coefficients and SFECT impedances of each plate were calculated. Fig. 5 shows the $\tilde{R}_{1,2}$ of the plates and a half space (the wave number is $\lambda_0 = 176.66(1/\text{meter})$ that the COIL-6's shape function is maximized, the same hereinafter). Since $\tilde{R}_{1,2} \approx R_{1,2}\left(1 - e^{-2k_2T_2}\right)$, where $R_{1,2}$ is the generalized reflection coefficient of a half space, the $\tilde{R}_{1,2}$ curves line up in order by T_2.

The change of generalized reflection coefficient, $\Delta\tilde{R}_{12} = \tilde{R}_{12} - \tilde{R}_{halfspace} \approx -R_{1,2}e^{-2k_2T_2}$, is plotted in Fig. 5(b). The modulus and phases of $\Delta\tilde{R}_{1,2}$ at arbitrary frequencies (999Hz and 5100Hz here) were plotted against thickness in Fig. 5(c). Both $\ln|\left(\Delta\tilde{R}_{1,2}\right)|$ and $\arg(\Delta\tilde{R}_{1,2})$are linearly correlated with T_2, whereas the slope of the curve changes with frequency. The aforementioned analytical example confirmed the logarithmic linear relation between $\Delta\tilde{R}_{1,2}$ and plate thickness.

What we measured, however, are impedance or voltage signals. Since the impedance is the integration of reflection coefficient and shape function, very likely it has a similar logarithmic linear relation with plate thickness. In the following investigation, we emulated a half space by an assumed 30mm thick plate, which is much thicker than the COIL-6's measureable thickness. The normalized impedance Z_{nor} [11], [17] of the 'half space' and the assumed plates were calculated using the equations elaborated in [11], [17] and [22]. The changes of normalized impedance from a half space, $\Delta Z_{nor}(= Z_{nor} - Z_{nor}|_{half\ space})$, are plotted in Fig. 6(a). Note the ΔZ_{nor} curves are similar in shape with the $\Delta\tilde{R}_{12}$ in Fig. 5(b) but 90 degrees rotated (note the complex operation, j, in Eq. (2)). The ΔZ_{nor} curves also line up in thickness order. The phases and amplitudes of ΔZ_{nor} at 999Hz and 5100Hz were calculated and plotted against T in Figs. 6(b). $\ln|(\Delta Z_{nor})|$ and $\arg(\Delta Z_{nor})$ change linearly with T.

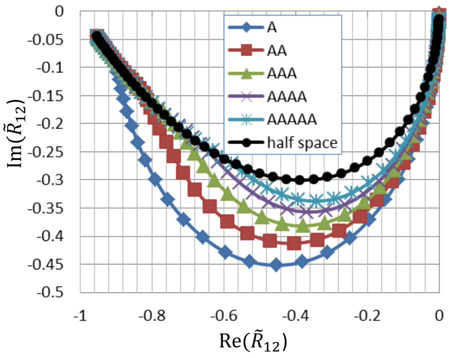

(a) The $\tilde{R}_{12}$

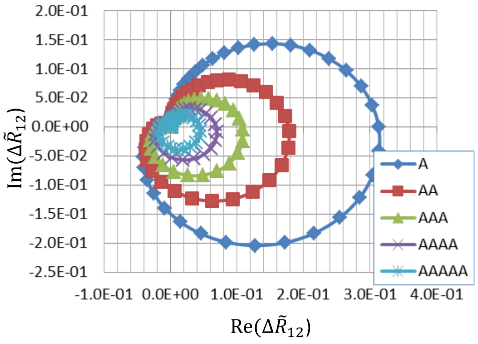

(b) The $\Delta\tilde{R}_{12}$

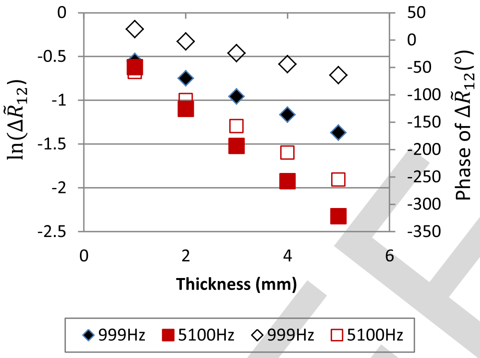

(c) Relation betw een log scaled $\Delta\tilde{R}_{12}$ and thickness

Fig. 5. Generalized reflection coefficient of single plate.

In order to elucidate the effects of material property described by Eq. (13), we made similar analytical investigation on assumed '***B***' plates whose conductivities are 1/5 of that of material '***A***'. Fig. 6(b) shows the change of the curve's slope with frequency and conductivity.

Hereto we analytically confirmed the linear relation between the novel characteristic features and a single plate's thickness. This linear relation is expected to lead to more accurate thickness assessment.

C. Reflection Coefficients of two-Plate Stacks

Fig. 7 shows a double-layered structure, a two-plate stack. Regions 1 and 4 are air; regions 2 and 3 are conducting slabs. The frequency responses are more complicated and the characterization is more difficult.

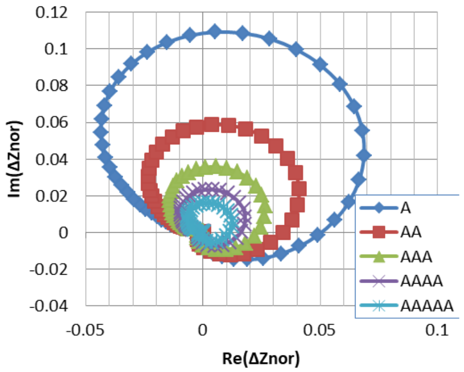

(a) ΔZ_{nor}

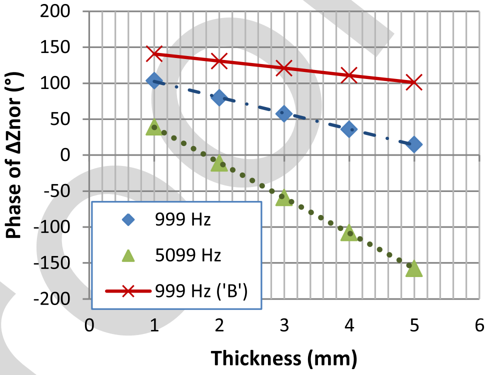

(b) Change of the phase of ΔZ_{nor}w ith thickness

Fig. 6. Change of normalized impedance and thickness.

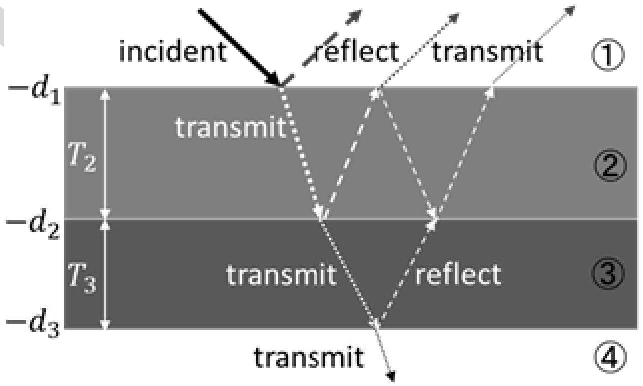

Fig. 7. Reflection and transmission of plane wave in eddy current measurement of a two-plate stack.

$\tilde{R}_{1,2}$ in (6) is also valid for a double-layered structure, whereas the $\tilde{R}_{2,3}$ is

$$\tilde{R}_{2,3} = \frac{R_{2,3} + \tilde{R}_{34} e^{-2k_3 T_3}}{1 + R_{2,3}\tilde{R}_{34} e^{-2k_3 T_3}} \cong \left(R_{2,3} + R_{34} e^{-2k_3 T_3}\right)\left(1 - R_{2,3} R_{34} e^{-2k_3 T_3}\right). \quad (13)$$

Note $\tilde{R}_{34} = R_{34}$ for double-layered structures.

Equation (13) indicates that $\tilde{R}_{23}$ is decided by the reflection between the two plates ($R_{2,3}$), the reflection between the lower layer and air (R_{34}), and the thickness of the lower layer (T_3), whereas

$$R_{2,3} = \frac{\mu_3 k_2 - \mu_2 k_3}{\mu_3 k_2 + \mu_2 k_3} = \frac{\mu_3^2 k_2^2 - \mu_2^2 k_3^2}{(\mu_3 k_2 + \mu_2 k_3)^2}$$

and

$$R_{3,4} = \frac{\mu_4 k_3 - \mu_3 k_4}{\mu_4 k_3 + \mu_3 k_4} = \frac{\mu_0 k_3 - \mu_3 \lambda_0}{\mu_0 k_3 + \mu_3 \lambda_0}. \qquad (14)$$

Obviously, if there is no difference between the two plates' material properties, $R_{2,3} = 0$, the double-layered structure merges into a single plate. If the two plates are of different electromagnetic properties, however, the sign of $R_{2,3}$ changes with $\mu_3^2 k_2^2 - \mu_2^2 k_3^2$. For non-ferromagnetic conductive materials,

$$R_{2,3} = \frac{j\omega\mu_0(\sigma_2 - \sigma_3)}{(k_2 + k_3)^2} \quad \text{and} \quad R_{3,4} = \frac{k_3 - \lambda_0}{k_3 + \lambda_0} = \frac{j\omega\mu_0\sigma_3}{(k_3 + \lambda_0)^2}. \qquad (15)$$

$R_{3,4}$ is always positive whereas the sign of $R_{2,3}$ is conductivity dependent: If the top layer is more conductive, $(\sigma_2 - \sigma_3) > 0$, then $R_{2,3} > 0$, consequently $\tilde{R}_{2,3} > 0$. In contrast, if the top layer is less conductive, $(\sigma_2 - \sigma_3) < 0$, then $R_{2,3} < 0$. Equation (13) indicates the sign of $\tilde{R}_{2,3}$ is determined by a relation between the magnitudes of $R_{2,3}$ and $R_{34}e^{-2k_3T_3}$: if $|R_{2,3}| > |\tilde{R}_{34}e^{-2k_3T_3}|$, $\tilde{R}_{2,3} < 0$; and vice versa.

The $\tilde{R}_{1,2}(= \frac{R_{1,2}+\tilde{R}_{2,3}e^{-2k_2T_2}}{1+R_{1,2}\tilde{R}_{2,3}e^{-2k_2T_2}})$ changes with $R_{1,2}$ and $\tilde{R}_{2,3}e^{-2k_2T_2}$. The percentage of the lower layer in the $\tilde{R}_{1,2}$ is determined by $\tilde{R}_{2,3}$ and the top layer's thickness T_2. The lower layer is shielded by a thick top layer but becomes more distinguishable at low frequencies, suggesting of characterizing lower layer using low frequency signals. Because $R_{1,2}$ is always negative in sign, if $(\sigma_2 - \sigma_3) > 0$ and the top layer is essentially thick, the amplitude of $\tilde{R}_{2,3}e^{-2k_2T_2}$ is smaller than that of $R_{1,2}$, $\tilde{R}_{1,2} = \frac{R_{1,2}+\tilde{R}_{2,3}e^{-2k_2T_2}}{1+R_{1,2}\tilde{R}_{2,3}e^{-2k_2T_2}} < 0$. In contrast, if $(\sigma_2 - \sigma_3) < 0$, the sign of $\tilde{R}_{2,3}$ is undetermined, neither that of $\tilde{R}_{1,2}$.

The change of $\tilde{R}_{1,2}$ from that of a half space, $\Delta\tilde{R}_{1,2}$, is defined by

$$\tilde{R}_{1,2} = \tilde{R}_{1,2} - R_{1,2} = \frac{R_{1,2} + \tilde{R}_{2,3}e^{-2k_2T_2}}{1 + R_{1,2}\tilde{R}_{2,3}e^{-2k_2T_2}} - R_{1,2}$$

$$\cong \left(1 - R_{1,2}^2\right)\tilde{R}_{2,3}e^{-2k_2T_2}\left(1 - R_{1,2}\tilde{R}_{2,3}e^{-2k_2T_2}\right). \qquad (16)$$

The real parts of $\left(1 - R_{1,2}^2\right)$ and $(1 - R_{1,2}\tilde{R}_{2,3}e^{-2k_2T_2})$ are larger than zero. If $(\sigma_2 - \sigma_3) > 0$, $\tilde{R}_{2,3} > 0$, as a result, $\mathrm{Re}(\Delta\tilde{R}_{1,2}) > 0$. However, if $(\sigma_2 - \sigma_3) < 0$, the sign of $\Delta\tilde{R}_{1,2}$ is undetermined.

The following are analytical examples to illustrate the theoretical inference in detail. Note the total thickness 'T_2+T_3' is limited to 6mm.

1) The top Layer Is More Conductive: $(\sigma_2 - \sigma_3) > 0$: Fig. 8(a) shows polar plots of $\tilde{R}_{1,2}$ of '$T_A + T_B'$ stacks that the conductivities of the top layer, σ_2, and lower layer, σ_3, are respectively 10MS/m and 2MS/m. The $\tilde{R}_{1,2}$ of single-layered $T_A$thick plates and 'half space' are also presented for comparison. As stated in the theoretical analysis, all $\tilde{R}_{1,2}$ are smaller than 0 and all the $\tilde{R}_{1,2}$ of layered structures are below that of a half space and line up in sequence by the top layer's thickness T_A. Furthermore, the $\tilde{R}_{1,2}$ of $'T_A + T_B'$ stacks are sandwiched between those of T_A mm and $(T_A + 1)$ mm thick single-layered plates made of material '***A***'.

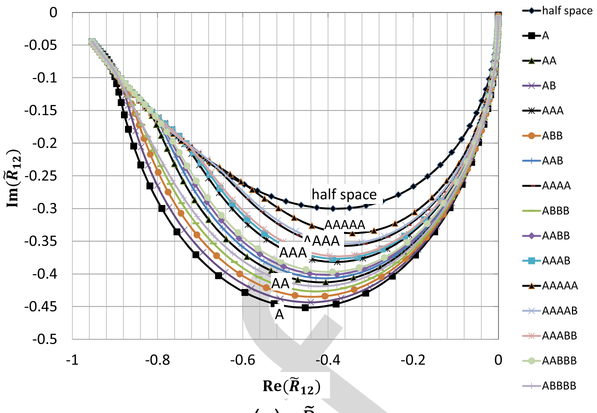

(a) $\tilde{R}_{1,2}$

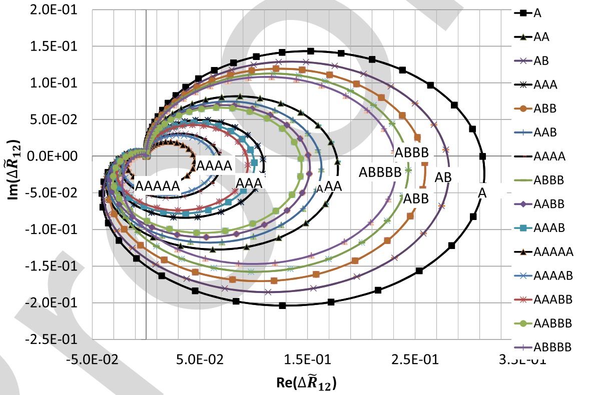

(b) $\Delta\tilde{R}_{1,2}$: the difference between a half space and '$T_A + T_B$' stack

Fig. 8. $\tilde{R}_{1,2}$ and $\Delta\tilde{R}_{1,2}$ of two-layered stacks that the top layer is more conductive.

Fig. 8(b) shows $\Delta\tilde{R}_{1,2}$, the change from a half space, are mainly in the 1st and the 4th quarters; almost all $\mathrm{Re}(\Delta\tilde{R}_{1,2})$ are of positive value. The $\Delta\tilde{R}_{1,2}$ curves of '$T_A + T_B'$ are also sandwiched between those of T_A mm and $(T_A + 1)$ mm thick single-layered '***A***' plates.

2) The top Layer Is Less Conductive: $(\sigma_2 - \sigma_3) < 0$: The top layer in a $T_B + T_A$ structure is less conductive, $(\sigma_2 - \sigma_3) < 0$. Fig. 9(a) shows $\tilde{R}_{1,2}$ of the '$T_B + T_A$' stacks and that of T_B thick single plates. Different from that of $T_A + T_B$, $\tilde{R}_{1,2}$ of $T_B + T_A$ are neither necessary below that of a half space, nor line up in order by thickness.

Fig. 9(b) shows that the $\mathrm{Re}(\Delta\tilde{R}_{1,2})$ of single T_B thick plates are generally larger than 0, whereas that of '$T_B + T_A$' are smaller than 0. The $\Delta\tilde{R}_{1,2}$ do not line up sequentially, implying difficulty in thickness estimation of '$T_B + T_A$'.

In either case, the generalized reflection coefficient of a double-layered structure is more complicated.

IV. EVALUATION OF A SINGLE PLATE'S THICKNESS

We applied the findings on $\Delta\tilde{R}_{1,2}$ and ΔZ_{nor} to evaluate a plate's thickness.

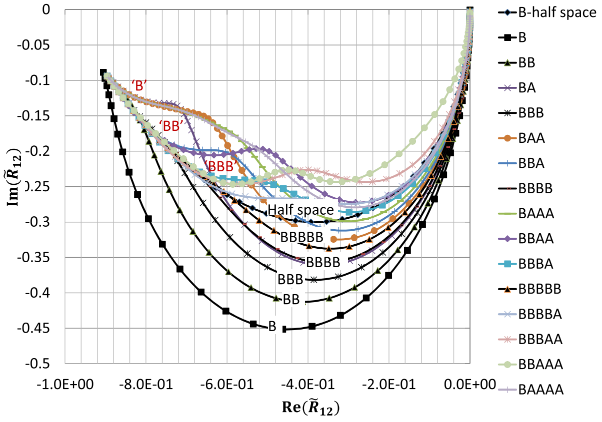

(a) $\tilde{R}_{12}$

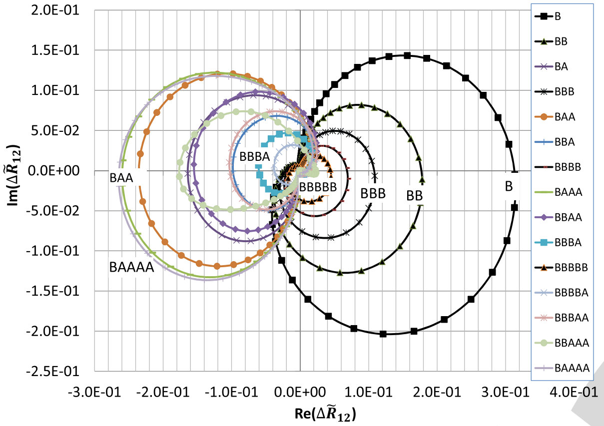

(b) $\Delta\tilde{R}_{12}$: the difference between a half space and '$T_B + T_A$' stack

Fig. 9. $\tilde{R}_{1,2}$ and $\Delta\tilde{R}_{1,2}$ of two layer stacks that the top layer is less conductive.

A. Analytical Study of Single Plate's Thickness Evaluation

In most practical circumstance, a test object's electromagnetic properties are unknown or inexact. The dependence of the characteristic features (section III B) on the frequency and material property (e.g., conductivity) impedes applying the linear relation (section III B) to practical inspection.

In [11] and [17], we analyzed the impedance signals Z_{nor} in terms of $\omega\sigma$ and used characteristic quantities, such as the minimum phase of Z_{nor} and maximum value of $R_{nor}(= \mathrm{Re}(Z_{nor}))$ in spectrum, to estimate the thickness of a conducting plate even without knowing its conductivity. This idea has been applied to $\Delta\tilde{R}_{1,2}$ and ΔZ_{nor} in this study.

In order to clarify the effect of conductivity, the Z_{nor} and ΔZ_{nor} of '***B***' plates were analyzed and compared to the ones of '***A***' plates. We calculated the logarithmic value of the maximum $|\Delta Z_{nor}|$, $\ln(|\Delta Z_{nor}|_{max})$, of each '***A***' and '***B***' plate and plot them against thickness T in Fig. 10(a). Despite the difference on conductivity, the $\ln(|\Delta Z_{nor}|_{max}) \sim T$ plots of '***A***' and '***B***' plates of same thickness coincide exactly, suggesting $\ln(|\Delta Z_{nor}|_{max})$ a proper characteristic feature to gauge the thickness of a plate even without knowing its conductivity.

By the way, because ΔZ_{nor} is the difference by frequency between the impedances of a plate of certain thickness and that of a half space, a significantly thick plate made of the same material of the one to be characterized is needed but not always available. Taking into account that for plates of same thickness, same $\omega\sigma$ yields same Z_{nor}, hence identical extrema in spectrum, such as $R_{nor}|_{max}$ and $Z_{nor}|_{\max(R_{nor})}$, we calculate the $\Delta Z_{nor}|_{\max(R_{nor})}$ of the to be characterized plate by referring to $Z_{nor}|_{\max(R_{nor})}$ of a 'half space' which is available in master curve construction. Fig. 10 (b) shows phases of $\Delta Z_{nor}|_{\max(R_{nor})}$ of '***B***' plates that respectively refer to 30mm thick '***A***' plate and 30mm thick '***B***' plate. The consistent of the phases (Fig. 10(b)) demonstrates the feasibility of gauging a single plate by referring to a master curve, even without knowing its conductivity nor having a 'half-space' made of the same material.

Comparing with the characteristic features taken from Z_{nor} [11, 17], the ones extracted from ΔZ_{nor} are highly linear with plate thickness. More accurate thickness measurement is expected.

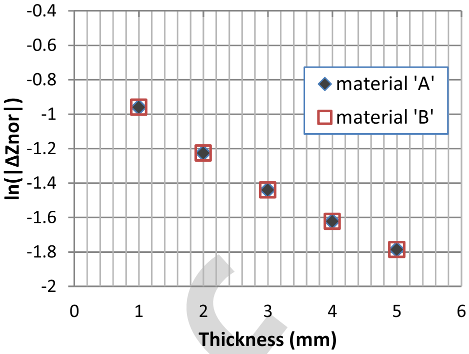

(a) Maximum of $\ln(\Delta Z_{nor})$ of plates made of materials '***A'*** and '***B'***.

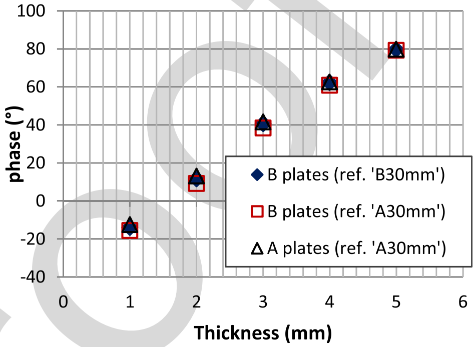

(b) Phase of ΔZ_{nor} when its real part is maximized, referred to 'half space' emulated respectively by '***A***' and '***B***' thick plates

Fig. 10. Identical of extrema over the spectrum of plates made of materials ***A*** and ***B***.

B. Experimental Verification of Single Plates' Thickness Evaluation

The experimental setup employed in [11] and [17] was adopted in this study. The COIL-6 was connected to an LCR meter (HIOKI, IM 3536 [23]) and filled with 10mA constant alternating current sweeping from 200Hz to 200kHz, with 300 equal intervals in log scale.

We measured the air-cored coil's impedance, $Z_{m0}(\omega)$, and the impedance of the coil coupling with test objects, $Z_m(\omega)$ (the subscript *m* stands for measurement and *0* for

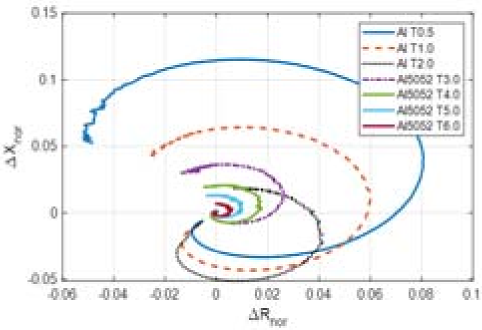

(a) ΔZ_{mnor} of Al and Al5052 plates

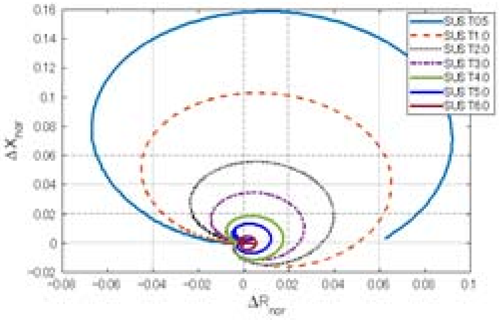

(b) ΔZ_{mnor} of SUS304 plates

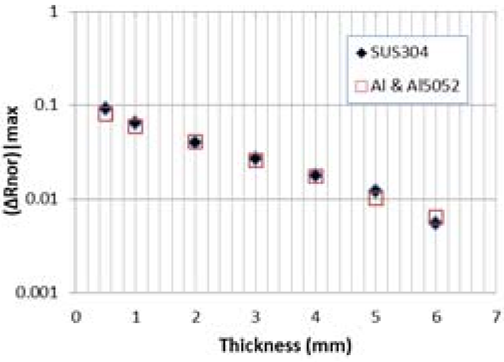

(c) Change of $\Delta R_{mnor}|_{max}$ with plate thickness.

Fig. 11. SFECT measurement signals of single plates.

test-object-free) and calculated the normalized impedance $Z_{mnor} = R_{mnor} + jX_{mnor}$ [11], [17]. The test objects are Aluminum plates (150mm(L)×150mm(W)×0.5mm/ 1mm/ 2mm (T)) and Aluminum alloy (Al5052) plates (150mm(L)×150mm(W)×3mm/ 4mm/5mm/ 6mm/8mm (T)). Because the measureable thickness of COIL-6 is 6mm, 'half space' was emulated by the 8mm thick Al5052 plate. ΔZ_{mnor} were calculated by referring to this 'half space'.

Fig. 11(a) shows the ΔZ_{mnor} of the Aluminum and Al5052 plates in the complex plane. The ΔZ_{mnor} of Aluminum plates shift from that of Al5052 plates because of difference on conductivities [17]. The maximum of real parts of ΔZ_{mnor}, $(\Delta R_{mnor})_{max}$, are plotted against the plate thickness in Fig. 11(c). The log scaled $(\Delta R_{mnor})_{max}$ is linearly correlated with thickness, despite the difference on Aluminum and Al5052.

Similar measurements were carried out on SUS304 plates (150mm(L)×150mm(W)×0.5mm/1.0mm/2.0mm/3.0mm/ 4.0mm/5.0mm//6.0mm (T)). The ΔZ_{mnor} of SUS 304 plates were calculated by referring to the 8mm thick Al5052 plate and plotted in Fig. 11 (b). The log scaled $(\Delta R_{mnor})_{max}$ are plotted against thickness in Fig. 11(c). The $(\Delta R_{mnor})_{max}$ of SUS304 plates is also a logarithmic linear function of plate thickness. This consistency demonstrates the conductivity independence of the relationship.

The experimental verification suggested the thickness of a single plate can be assessed by using the conductivity independent correlation between $(\Delta R_{mnor})_{max}$ and thickness.

V. EVALUATION OF DOUBLE-LAYERED STRUCTURES

The thicknesses of two closely attached plates in a double-layered structure were evaluated using one set of SFECT signals.

A. Analytical Study: the Derivative of Z_{nor} With Respect to Log Scaled Angular Frequency

We characterized two air-gap-separated layers using low frequency and high frequency signals in [10]. The signals of two closely attached plates (Fig. 7) are more difficult to separate.

Figs. 8(a) and 9(a) demonstrate the merging of $\tilde{R}_{12}$ of structures with same top layer at high frequencies. Same behaviors are for Z_{nor} and related quantities, such as the phase of Z_{nor} (Figs. 12(a) and 12(b)). Fig. 12 also shows the merging of '$T_B + T_A$' signals occurs at higher frequencies than that of '$T_A + T_B$' because of lower conductivity of material '***B***'. Fig. 12(a) shows a minimum in the phase spectrum of a '$T_A + T_B$' structure. For a '$T_B + T_A$' stack, however, Fig. 12(b) shows a local minimum followed by a local maximum at higher frequencies in the spectrum.

The minimum phases of Z_{nor} of '$T_A + T_B$' structures were taken from Fig. 12(a) and plotted with respect to the constituent in Fig. 13, showing the increase of $phase|_{min}$ with T_B for the stacks with same top layer. In other words, given the top layer's thickness, the lower layer's thickness T_B could be assessed properly (Fig. 13). However, Fig. 12(a) shows no clue on how to find out the top layer's thickness.

For '$T_B + T_A$' structures, the highly conductive '***A***' layer cannot be completely shielded by a thin top layer (e.g., $T_B = 1mm$) so that T_A could be determined by referring to a relation between the phase of Z_{nor} and T_A. However, in the case of a thick top layer, the lower layer is deeply shielded. We have to turn to more sensitive quantities.

The derivative of Z_{nor} with respect to log scaled angular frequency ($\Omega = \log\omega$), $\frac{\partial Z_{nor}}{\partial \Omega}(= \omega\frac{\partial Z_{nor}}{\partial \omega})$, physically represents the Z_{nor} per unit of Ω. The difference of Z_{nor} in the log scaled frequency series, $d_f(Z_{nor})$, is defined by

$$\begin{aligned} d_f(Z_{nor})|_i &= Z_{nor}|_{i+1} - Z_{nor}|_i \\ &= (d_f(R_{nor}) + j d_f(X_{nor}))|_i, \quad (\text{i}=1, \text{N-1}) \end{aligned} \tag{17}$$

where N is the number of discrete frequencies (N = 60 in the analytical study). Because $\Delta\Omega$ is same for equally distanced log scaled frequencies, $d_f(Z_{nor})$ has similar physics meaning

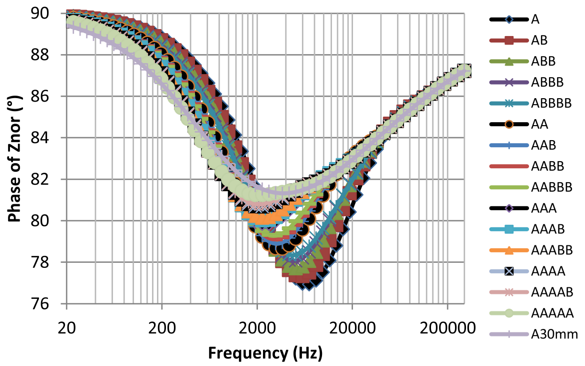

(a) Phase of '$T_A + T_B$' structure

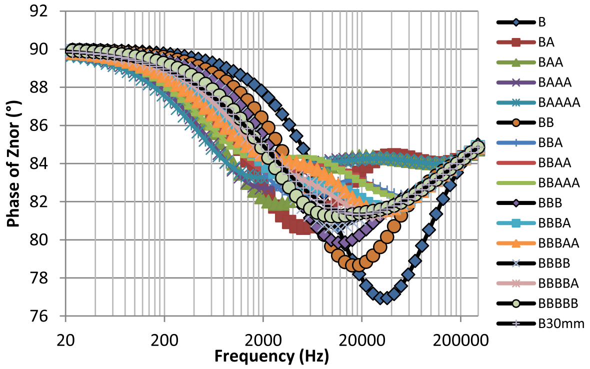

(b) Phase of "$T_B + T_A$' structure

Fig. 12. Phases of Z_{nor} of double layered structures.

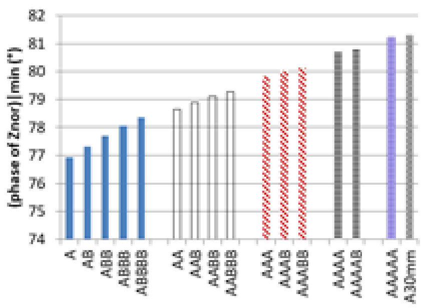

Fig. 13. Extreme values (minimum Phase of Z_{nor}) of '$T_A + T_B$' structure.

as $\frac{\partial Z_{nor}}{\partial \Omega}$: the change of Z_{nor} with respect to every unit change in Ω.

By the way, if $Z_{nor}(\omega) = |Z_{nor}|e^{j\omega} = R_{nor}(\omega) + jX_{nor}(\omega)$, then

$$\frac{\partial Z_{nor}}{\partial \omega} = j|Z_{nor}|e^{j\omega} = jZ_{nor}(\omega). \tag{18}$$

It implies the exchange of the real and imaginary parts' properties of $Z_{nor}(\omega)$ and $\frac{\partial Z_{nor}}{\partial \omega}$. Although $|Z_{nor}|$ could be a function of ω so that $\frac{\partial Z_{nor}}{\partial \omega}$ might be in a more complicated form, (18) gives hints on the relation between $Z_{nor}(\omega)$ and $\frac{\partial Z_{nor}}{\partial \Omega}$, e.g., characteristics of $\mathrm{Re}(Z_{nor})$ might appear in $\mathrm{Im}(\frac{\partial Z_{nor}}{\partial \Omega})$.

As examples, Figs. 14 (a) and 14(b) show respectively Z_{nor} and $d_f(Z_{nor})$ of stacks whose top layer $T_B = 2mm$ (denoted by 'BB' in Fig.14). Both Z_{nor} and $d_f(Z_{nor})$ merge in the high frequency areas (enclosed by dotted ellipses), whereas extrema appear in the areas enclosed by solid line. Note the difference on lower layer exhibits in the real part of Z_{nor} (Fig. 14(a)) but imaginary part of $d_f(Z_{nor})$ (Fig. 14(b)). Hereafter we seek characteristic quantities from the spectrum of $d_f(Z_{nor})$ for thickness evaluation.

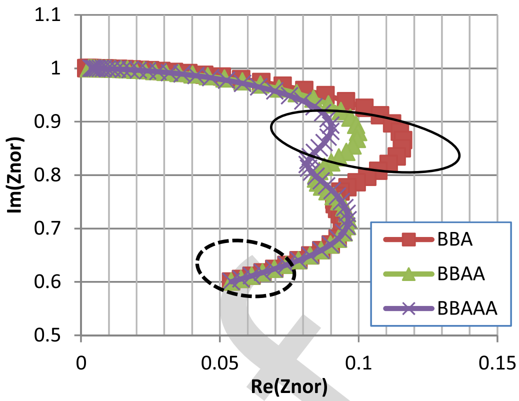

(a) Z_{nor} of 'BB*' stacks

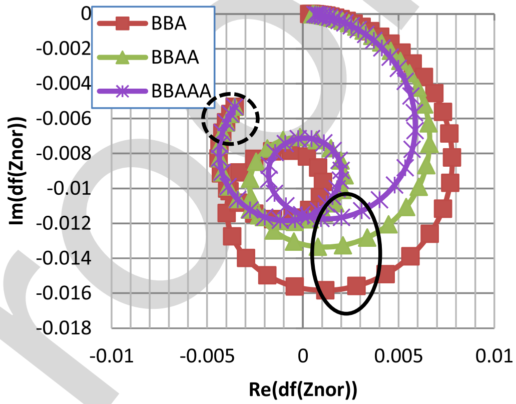

(b) $d_f(Z_{nor})$ of 'BB*' stacks

Fig. 14. Complex plane plots of Z_{nor} and $d_f(Z_{nor})$ of double layered structure '$T_B + T_A'$ that $T_B = 2$mm.

1) Thicknesses of Layers in a '$T_A + T_B$' Stack: Fig. 15 (a) shows the phases of $d_f(Z_{nor})$ of '$T_A + T_B$' structures. We took the local maximal phase in high frequency range (enclosed by the dotted line) and plotted them against T_A in Fig. 15(b). The diamond and error bar represent the average and standard deviation of the maximal phases of '$T_A + T_B$' structures with same T_A. The ones of single T_A thick plates are also presented. Fig. 15(b) shows the local maximal phase appearing in high frequency range is mainly decided by the top layer's thickness T_A, thereby T_A can be assessed using this feature. The minimal of the imaginary part of $d_f(Z_{nor})$ were taken from the spectrum and plotted against the lower layer's thickness in Fig. 15(c). For structures with same top layer, the minimum $\mathrm{Im}(df(Z_{nor}))$ increases with lower layer's thickness. Therefore, we can find out the top layer's thickness T_A by referring to the local maximal phase of $df(Z_{nor})$ in high frequency range (Fig. 15(b)), and then have the lower layer's thickness T_B by referring to the minimum phase of Z_{nor} (Fig. 13) or minimal $\mathrm{Im}(df(Z_{nor}))$ (Fig. 15(c)).

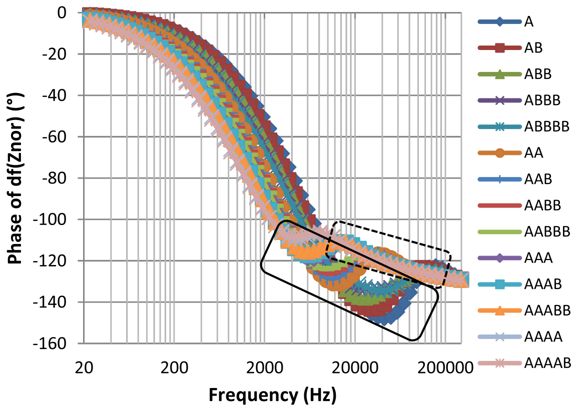

(a) Phases of the $d_f(Z_{nor})$ of '$T_A + T_B$' structures

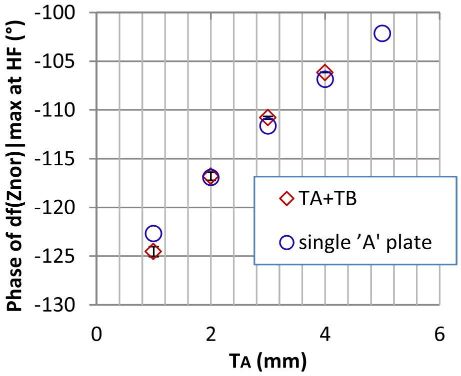

(b) The maximum of $d_f(Z_{nor})$ phases in high frequency range

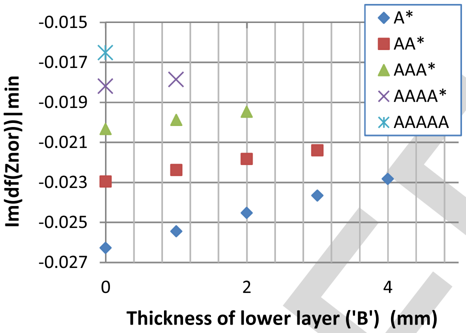

(c) The minimum of $\mathrm{Im}(d_f(Z_{nor}))$ in the spectrum

Fig. 15. Phases of $d_f(Z_{nor})$ of '$T_A + T_B$' structures (HF: High Frequency).

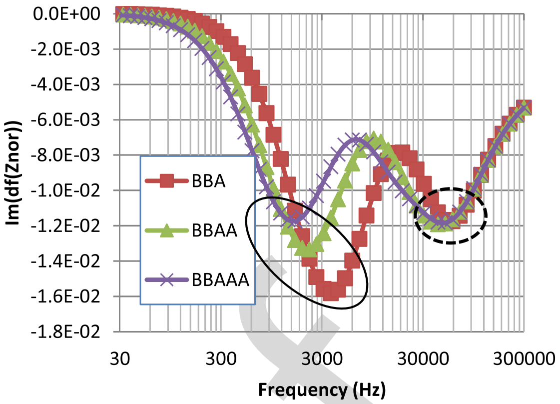

(a) Imaginary part of the $d_f(Z_{nor})$

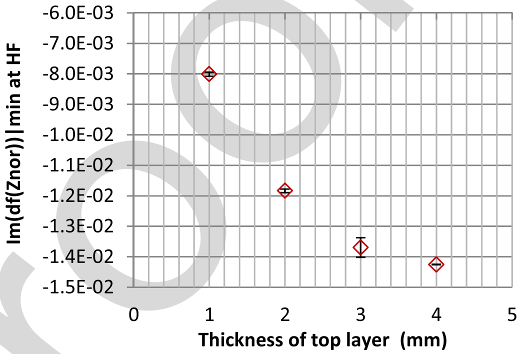

(b) The minimal of Im($d_f(Z_{nor})$) in high frequency range

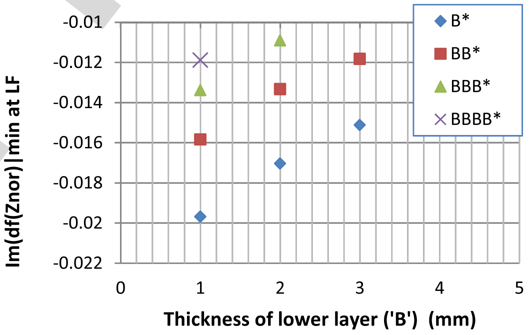

(c) The minimal of $\mathrm{Im}(d_f(Z_{nor}))$ in low frequency range

Fig. 16. Characteristic features taken from $d_f(Z_{nor})$ for thickness estimation of '$T_B + T_A$' stacks (HF: High Frequency; LF: Low Frequency).

2) Thicknesses of Layers in a '$T_B + T_A$' Stack: As an example, the spectrum of $\mathrm{Im}(d_f(Z_{nor}))$ of '$T_B + T_A$' stacks that $T_B = 2mm$ is presented in Fig. 16(a). Local minimums appear respectively in high frequency and low frequency ranges (enclosed by dotted line and solid line ellipses). The minimal values of all the possible constituents were taken. Fig. 16(b) shows the average and standard deviation of minimal $\mathrm{Im}(d_f(Z_{nor}))$ in high frequency range for structures with same top layer. This quantity decreases with top layer's thickness, and the deviation is very small, suggested a valid characteristic feature to estimate top layer's thickness. Fig. 16(c) shows the minimal taken from the low frequency range increases with lower layer's thickness, for stacks with same top layer. Figs. 16(b) and 16(c) suggested that the two local minimal values are characteristic quantities for thickness evaluation: the one appears in the high frequency range is for top layer's thickness T_B and the one in the lower frequency range is for the lower layer's thickness T_A.

In summary, we can estimate the thicknesses of two closely attached plates by using the Z_{nor} or $\mathrm{d}_f(Z_{nor})$ related quantities. The top layer's thicknesses can be estimated by referring to $\mathrm{d}_f(Z_{nor})$ related extrema appearing at high frequencies, and the lower layer's thickness by using extrema of Z_{nor} or $\mathrm{d}_f(Z_{nor})$ appearing at lower frequencies thereafter.

B. Experimental Verification of SFECT Measurement of Two-Plate Stacks

Two-plate stacks were formed by SUS304, Al5052 alloy and Aluminum plates whose conductivities increase sequentially. The total thickness of a two-plate stack is limited to 6mm. Table II shows the possible constituents.

TABLE II
CONSTITUENTS OF TWO-PLATE STACKS

		Aluminum (mm)			Al5052 (mm)		
		0. 5	1	2	3	4	5
SUS304 (mm)	0.5	○	○	○	○	○	○
	1	○	○	○	○	○	○
	2	○	○	○	○	○	
	3	○	○	○	○		
	4	○	○	○			
	5	○	○				

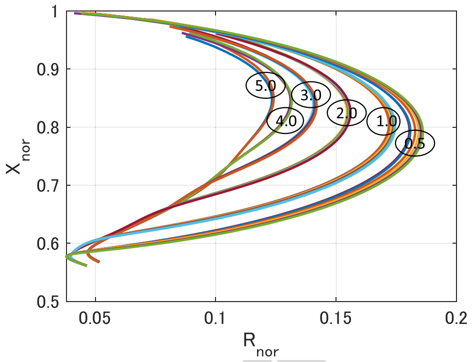

(a) Z_{nor}

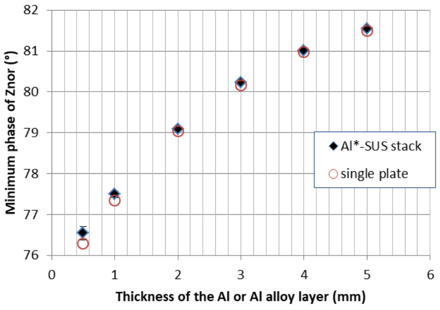

(b) The minimum phase of Z_{nor} and the top layer thickness

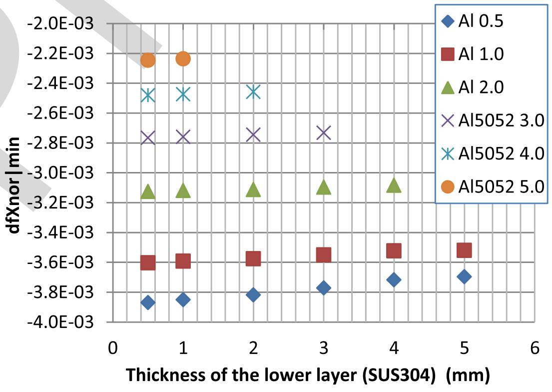

(c) Change of the minimum value of $d_f(X_{nor})$ with the lower layer thickness

Fig. 17. Measurement of two-plate stacks that the top layer is more conductive.

The same measurement setting for single-layered plate was employed.

1) The Top Layer Is More Conductive: A two-plate stack whose top layer is more conductive was formed by placing a piece of Aluminum or Al5052 plate on a SUS304 plate.

Fig. 17(a) shows the grouping of Z_{mnor} by top layer's thickness. The number in circle indicates the top layer's thickness in mm. The minimum in the spectrum of the phase of Z_{nor} were taken. The average and standard deviation of the phases of the two-plate stacks with same top layer were calculated and denoted by diamond and error bar in Fig. 17(b). Fig. 17(b) also shows the minimum phases of single-layered plates (denoted by hollow circle). The measurement results are very similar to the analytical results (Fig. 15(b)). Note the 0.5mm, 1mm and 2mm thick top layers are made of Aluminum and the ones thicker than 3mm are made of Al5052. The correlation shown in Fig. 17(b) implies the independency of this characteristic feature on top layer's conductivity.

We investigated the frequency response of $d_f(Z_{nor})$ to evaluate the lower layer's thickness. Fig. 17(c) shows, for stacks with same top layer, the minimum of the Im($d_f(Z_{nor})$) increases with lower layer's thickness. The slight difference in the $d_f(X_{nor})|_{min}$ of stacks with thick top layers (e.g., 4mm, 5mm) also shows the difficulty in measuring the lower layer.

The experimental results demonstrated the possibility of finding out the top Aluminum or Al5052's plate's thickness by referring to the minimum phase of Z_{nor} (Fig. 17(b)), and thenceforth estimate the lower SUS304 layer's thickness by referring to the minimum of Im($d_f(Z_{nor})$). Note these characteristic features are conductivity independent. In other words, the thickness of the layers can be evaluated even without knowing their conductivities.

2) The Top Layer Is Less Conductive: A two-plate stack whose top layer is less conductive is formed by exchanging the position of the two plates in 1).

Fig. 18(a) shows the Z_{mnor} of this type of two-plate stacks are very complicated. We calculated the $d_f(Z_{mnor})$ and analyzed the frequency response of related variables. Fig. 18(b) shows the spectrum of Im($d_f(Z_{mnor})$) of stacks with 2.0mm thick SUS304 top layer. There are local minimal values in the spectrum of $d_f(X_{nor})$: The one in high frequency range is relevant to the top SUS304 layer, whereas the one appearing in low frequency range corresponds to both layers.

The average and standard deviation of minimums in the high frequency range of stacks with same SUS304 top layer were calculated and presented in Fig. 18(c), showing the minimum of $d_f(X_{nor})$ in the high frequency range decreases with the SUS304 layer's thickness. The standard deviation is very small. In other words, the minimal Im($d_f(Z_{nor})$) in the high frequency range is a characteristic feature to evaluate the top layer's thickness. Note the frequency used in this study is not high enough to characterize 0.5mm and 1.0mm thick top layers made of SUS304.

The minimum of $d_f(X_{nor})$ in lower frequency range were extracted and plotted against the lower layer's thickness in Fig. 18(d). This characteristic quantity increases with lower layer's thickness for stacks with same top layer. By the way, the smooth change of $d_f(X_{nor})$ with lower layer's thickness, regardless of the difference on material (Aluminum for plates thinner or equal to 2mm, and Al5052 for plates thicker or equal

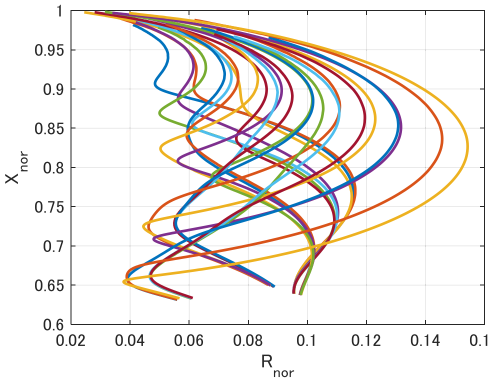

(a) Z_{nor}

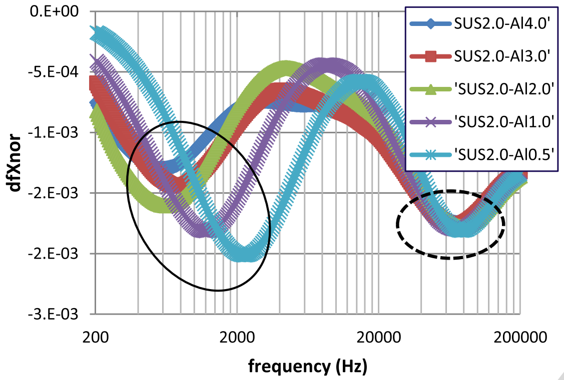

(b) Frequency response of $d_f(X_{nor})$

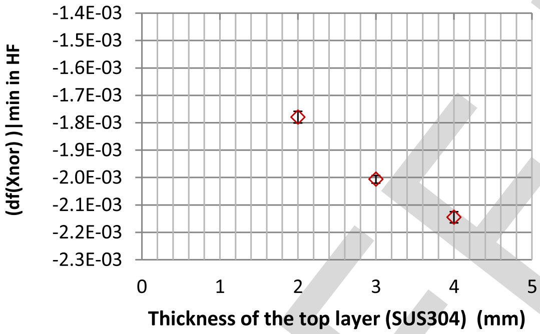

(c) Minimal of $d_f X_{nor}$ in high frequency range

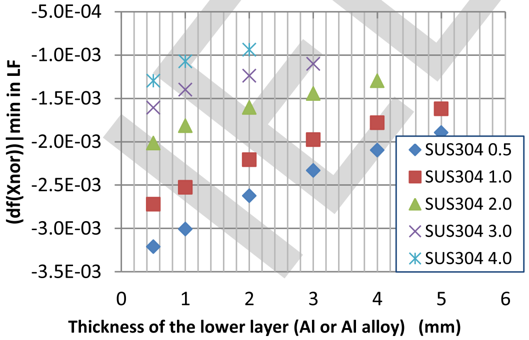

(d) Change of the minimum of df(Xnor) in low frequency range with the lower layer's thickness.

Fig. 18. Measurement of two-plate stacks that the top layer is less conductive. (LH: low frequency; HF: high frequency).

to 3mm), implying the conductivity independent of this feature..

The experimental verification suggests the feasibility of finding out the top layer's thickness by using the minimal of $\mathrm{Im}(d_f(Z_{nor}))$ in high frequency range (Fig. 18(c)), and the lower layer's thickness by using minimal of $\mathrm{Im}(d_f(Z_{nor}))$ in low frequency range (Fig. 18(d)). The thickness estimation is conductivity independent.

VI. CONCLUSIONS

Prior work has showed it is possible to measure a single conductive plate's thickness regardless of the plate's conductivity by SFECT. In this study we improved and extended the existed work in three aspects: selecting a suitable probe for a given object; enhancing the accuracy of thickness estimation by finding out characteristic features linearly correlated with thickness, and ultimately determining the thickness of each layer in a double-layered structure.

The impedance signals are integrand of shape function and reflection coefficient. Analytical study showed the wavelength that maximizes the shape function is an indicator of an air-cored coil's thickness measurement ability, and was introduced as a criteria for selecting a suitable probe for a given test object.

Theoretical inference showed the generalized reflection coefficient of a layered structure could be considered a modification of that of a half space, similar is the impedance signal. The logarithmic linear relation between the modification and plate thickness inferred more accurate thickness evaluation.

With regard to a double-layered structure, the signal also depends on the relation between the two layer's conductivities. For the characterization of two closely attached layers, we introduced a variable equivalent to the derivative of Z_{nor} with respective to log scaled angular frequency, that is, the difference of Z_{nor} in the equally distanced log scaled frequency series, $d_f(Z_{nor})$. Spectral analysis showed the extremum of $d_f(Z_{nor})$ in high frequency range is relevant to the top layer and therefore a characteristic feature to gauge the top layer's thickness, whereas the extremum, such as the phase or magnitude of the imaginary parts, appear in lower frequency range are relevant to both the top and lower layers. Given the top layer's thickness, the lower layer can be assessed accordingly. The findings were experimentally verified.

So far, we provided an approach to determine layers' thicknesses regardless of the layer-wise conductivities by spectral analysis of SFECT. In this study, the number of closely attached conductive layers is limited to two. The number of layers and the margin of difference between the conductivities are other concerns that need to be clarified in future studies.

REFERENCES

[1] Y. Zhao, X. M. Li, L. Lin, and M. K. Lei, "Measurements of coating density using ultrasonic reflection coefficient phase spectrum," *Ultrasonics*, vol. 51, no. 5, pp. 596–601, Jul. 2011.

[2] Y. Zhao, L. Lin, X. M. Li, and M. K. Lei, "Simultaneous determination of the coating thickness and its longitudinal velocity by ultrasonic nondestructive method," *NDT E Int.*, vol. 43, no. 7, pp. 579–585, 2019.

[3] Z. Y. Ma, W. Zhang, Z. B. Luo, L. Lin, and S. Krishnaswamy, "Thickness determination of dual-layer coatings based on ultrasonic spectral filtering," *Insight*, vol. 60, no. 4, pp. 200–205, Apr. 2018.

[4] P. Neumaier, *Simultaneous Thickness Measurement of Paint and Zinc Coatings in the Automotive Industry* (Duplex Corrosion Protection). Athens, AL, USA: Surface World, 2010, pp. 28–34.

[5] X.-Z. Gong, L. Cheng, and F.-H. Yu, "Multilayer thin film thickness measurement using sensitivity separation method," *Opt. Commun.*, vol. 283, no. 20, pp. 3989–3993, Oct. 2010.

[6] W. Yin and A. J. Peyton, "Thickness measurement of non-magnetic plates using multi-frequency eddy current sensors," *NDT E Int.*, vol. 40, no. 1, pp. 43–48, Jan. 2007.

[7] C.-C. Tai, "Characterization of coatings on magnetic metal using the swept-frequency eddy current method," *Rev. Sci. Instrum.*, vol. 71, no. 8, pp. 3161–3167, Aug. 2000.

[8] W. Cheng, "Pulsed eddy current testing of wall-thinning through insulation and cladding," *J. Nondestruct. Eval.*, vol. 31, no. 3, pp. 40–45, 2012.

[9] M. Pan, Y. He, G. Tian, D. Chen, and F. Luo, "PEC frequency band selection for locating defects in two-layer aircraft structures with air gap variations," *IEEE Trans. Instrum. Meas.*, vol. 62, no. 10, pp. 2849–2856, Oct. 2013.

[10] W. Cheng and H. Hashizume, "Characterization of multilayered structures by swept-frequency eddy current testing," *AIP Adv.*, vol. 9, no. 3, Mar. 2019, Art. no. 035009, doi: 10.1063/1.5079959.

[11] W. Cheng, "Thickness measurement of metal plates using swept-frequency eddy current testing and impedance normalization," *IEEE Sensors J.*, vol. 17, no. 14, pp. 4558–4569, Jul. 2017, doi: 10.1109/JSEN.2017.2710356.

[12] Z. Chen, L. Janousek, N. Yusa, and K. Miya, "A nondestructive strategy for the distinction of natural fatigue and stress corrosion cracks based on signals from eddy current testing," *J. Pressure Vessel Technol.*, vol. 129, no. 4, pp. 719–728, Nov. 2007.

[13] Z. Chen, M. Rebican, N. Yusa, and K. Miya, "Fast simulation of ECT signal due to a conductive crack of arbitrary width," *IEEE Trans. Magn.*, vol. 42, no. 4, pp. 683–686, Apr. 2006.

[14] L. U. Daura and G. Y. Tian, "Wireless power transfer based non-destructive evaluation of cracks in aluminum material," *IEEE Sensors J.*, vol. 19, no. 22, pp. 10529–10536, Nov. 2019.

[15] A. Sophian, G. Tian, and M. Fan, "Pulsed eddy current non-destructive testing and evaluation: A review," *Chin. J. Mech. Eng.*, vol. 30, no. 3, pp. 500–514, 2017.

[16] G. Y. Tian, Y. He, I. Adewale, and A. Simm, "Research on spectral response of pulsed eddy current and NDE applications," *Sens. Actuators A, Phys.*, vol. 189, pp. 313–320, Jan. 2013.

[17] W. Cheng, "Swept-frequency eddy current testing to characterize a nonmagnetic metallic plate and a nonconductive coating over it," *Intl. J. Appl. Electromagn. Mech.*, vol. 59, no. 14, pp. 1169–1178, Nov. 2018, doi: 10.3233/JAE-171129.

[18] M. Fan, P. Huang, B. Ye, D. Hou, G. Zhang, and Z. Zhou, "Analytical modeling for transient probe response in pulsed eddy current testing," *NDT E Int.*, vol. 42, no. 5, pp. 376–383, Jul. 2009.

[19] D. J. Harrison, "Characterisation of cylindrical eddy-current probes in terms of their spatial frequency spectra," *IEE Proc.-Sci., Meas. Technol.*, vol. 148, no. 4, pp. 183–186, Jul. 2001.

[20] C. P. Dolabdjian, L. Perez, V. O. De Haan, and P. A. De Jong, "Performance of magnetic pulsed-eddy-current system using high dynamic and high linearity improved giant MagnetoResistance magnetometer," *IEEE Sensors J.*, vol. 6, no. 6, pp. 1511–1517, Dec. 2006.

[21] W. C. Chew, *Waves and Fields in Inhomogeneous Media*. Piscataway, NJ, USA: IEEE Press, 1994, pp. 49–52.

[22] T. P. Theodoulidis, E. E. Kriezis, *Eddy Current Canonical Problems* (With Applications to Nondestructive Evaluation), 1st ed. New York, NY, USA: Tech Science Press, 2006.

[23] *User's Manual of IM3536 LCR Meter*, (in Japanese), 2nd ed. HIOKI, Nagano, Japan, Sep. 2016.

Weiying Cheng received the B.S. and M.S. degrees in electrical engineering from Zhejiang University, Hangzhou, China, in 1988 and 1991, respectively, and the Ph.D. degree in quantum engineering and systems science from the University of Tokyo, Tokyo, Japan, in 2000.

From 1991 to 1996, she was a Lecturer with the Department of Electrical Engineering, Zhejiang University. From 2000 to 2002, she was a Researcher with the Science Solutions International Laboratory, Tokyo. Since 2002, she has been a Principal Researcher with NDE Center, Japan Power Engineering and Inspection Corporation, Yokohama, Japan. Her research interests include the numerical modeling and simulation, data analysis, signal processing, and nondestructive testing and evaluation.

Dr. Cheng is a member of the Institute of Electrical Engineering of Japan, the Japan Society of Non-destructive Inspection, and the Japan Society of Maintenance.

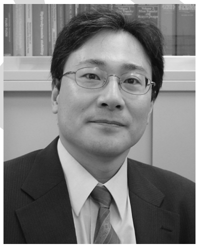

Hidetoshi Hashizume received the B.S., M.S., and Ph.D. degrees in nuclear engineering from the University of Tokyo, Japan.

From 1986 to 1991, he was a Research Assistant and an Assistant Professor with the University of Tokyo. Since 1991, he has been an Associate Professor with the Nuclear Engineering Department, Tohoku University, Sendai, Japan. From 1999, he is a Professor with Tohoku University. His research interests include HTc superconducting magnet system, MHD flow control, and NDT based on electromagnetic phenomena.